
Article:
Hurrell, A., Horoshenkov, K.V. orcid.org/0000-0002-6188-0369, King, S.G. et al. (1 more author) (2021) On the relationship of the observed acoustical and related non-acoustical behaviours of nanofibers membranes using Biot- and Darcy-type models. Applied Acoustics, 179. 108075. ISSN 0003-682X

https://doi.org/10.1016/j.apacoust.2021.108075

Applied Acoustics 179 (2021) 108075

Contents lists available at ScienceDirect

Applied Acoustics

journal homepage: www.elsevier.com/locate/apacoust

On the relationship of the observed acoustical and related non-acoustical behaviours of nanofibers membranes using Biot- and Darcy-type models

A. Hurrell [a,*], K.V. Horoshenkov [a], S.G. King [b], V. Stolojon [b]

[a] Department of Mechanical Engineering, University of Sheffield, Western Bank, Sheffield S1 3JD, UK
[b] Advanced Technology Institute, Department of Electrical and Electronic Engineering, University of Surrey, Guildford, Surrey GU2 7XH, UK

ARTICLE INFO

Article history:
Received 12 October 2020
Received in revised form 25 January 2021
Accepted 26 March 2021

ABSTRACT

There is a general lack of publications on the acoustical and related non-acoustical properties of nanofibrous media. This work attempts to contribute to this gap and to highlight problems associated with acoustic and related non-acoustic characterisation of these materials. The work, presumably for the first time, applies Biot- and Darcy-type mathematical models to explain the observed acoustical and related non-acoustical behaviours of the nanofibres. It identifies theoretical gaps related to the physical phenomena which can be responsible for the observed acoustical behaviours of nanofibrous membranes and it presents recommendations to fill these gaps. The novelty of this work is in the use of a robust theoretical model to explain the measured acoustical behaviour of thin nanofibrous membranes placed on a foam substrate. With this model the actual flow resistivity of nanofibers is estimated from acoustical data. It is demonstrated that a classical model for the flow resistivity of fibrous media does not work when the Knudsen number becomes greater than 0.02, i.e. then the diameter of nanofibres becomes comparable with the mean free path.

1. Introduction

Acoustic absorbers are commonly used to control sound levels for user comfort, meet regulatory specification or to provide audio privacy between domestic or commercial spaces. Typically, these absorbers come in the form of layers of foam or glasswool. In order to control efficiently levels of low frequency sounds, e.g. engine noise in a car or aircraft, a relatively thick layer of porous material is required. As a result, there is a clear need to find more environmentally friendly, lighter, and thinner absorbers which meet the acoustic performance specifications.

One promising material which can achieve high acoustic absorption performance with a relatively thin porous layer is nanofibre. Nanofibrous non-woven materials are typically comprised of a chosen polymer and fabricated using methods such as electrospinning. These fibres are comprised of randomly oriented infinitely long webs and their thickness is typically about 500 times smaller than that of the human hair, i.e. much less than 1μm. The nanosized diameter of the fibres results in the final material possessing a significantly higher surface area and resistivity to air flow, giving rise to acoustic absorption which is not achievable with traditional foams or fibrous media.

However, the understanding of the underpinning science behind nanofibrous materials in acoustics is limited. Modelling the acoustical and non-acoustical properties of nanofibrous membranes is particularly challenging for two reasons. Firstly, there are numerous difficulties associated with the characterisation of key intrinsic material parameters of the membranes, such as membrane thickness, density, and pore size. Secondly, these membranes typically lack sufficient thickness and high enough levels of stiffness to be tested for their acoustical properties using a standard method. As a result, there is a general lack of publications on the acoustical and related non-acoustical properties of nanofibrous media. Existing publications typically present scanning electron microscope (SEM) images of these media together with the acoustic absorption coefficient or transmission loss data (e.g. [1,2]). These works often, at length, discuss the nanofibre production process, quote data on the fibre diameters and measure surface densities for the nanofibrous membranes produced. However, little or no information is usually presented on the material pore structure, membrane thickness or bulk density. No effort is made to explain the observed acoustical performance of nanofibrous membranes using a valid theoretical or semi-empirical model [1,2].

This paper attempts to provide a better understanding of the link between the material characteristics of nanofibers and their acoustical properties. It also describes the problems associated with acoustic and related non-acoustic characterisation of these

* Corresponding author
E-mail address: aihurrell@gmail.com (A. Hurrell).

https://doi.org/10.1016/j.apacoust.2021.108075
0003-682X/

materials. It uses, probably for the first time, Biot- and Darcy-type mathematical models to explain the observed acoustical and related non-acoustical behaviour of nanofibres. It identifies theoretical gaps related to the physical phenomena which can be responsible for the observed acoustical behaviour of nanofibrous membranes and it makes recommendations to fill these gaps.

2. Material preparation

Poly(methyl methacrylate) (PMMA), 120,000 M_w, Acetic Acid, and Formic Acid were all purchased from Sigma-Aldrich (Sigma-Aldrich, MI, USA) and used as received. Poly(ethyleneterephthalate) (PET) was purchased from Sigma-Aldrich in granular form, with 30% glass particles as a stabiliser. During SEM analysis, the glass stabilisers were not observed to visibly impact the formation of fibres in electrospinning and exist only to stabilise the polymer in its granular form. The glass stabilisers are not chemically bound to the polymer [16]. The PET granules were dissolved into trifluoroacetic acid (TFA), 99% reagent grade, sourced from Alfa Aesar (Alfa-Aesar, MA, USA). Poly(ε-caprolactone) (PCL), 14,000 M_w, was purchased from Sigma-Aldrich, and dissolved in a ratio of 90:10 dimethylcarbonate (DMC): dimethylformamide (DMF) at a concentration of 10% w/v. DMC and DMF were purchased from Sigma-Aldrich, 99% reagent grade. The melamine foam used was an open cell material produced by BASF (BASF, Ludwigshafen, GER), marketed as Basotect G+, and supplied by Foam Techniques Ltd.

The membrane samples were electrospun using in-house built single-needle electrospinning rigs at the University of Surrey and the University of Sheffield. Pump-rates were tailored to each solution, voltage, and atmospheric conditions, increasing the rate to the maximum possible before unwanted dripping from the spinneret was observed. This ensured a stable, steady stream of polymer for optimum nanofibre production.

The PMMA nanofibres produced by the University of Surrey were done so with solutions being pumped to the spinneret using a Chemyx OEM syringe pump at rates between 500-2000 μl/hour. The spinneret was charged to 15 and 21 kV using a Glassman power supply, positioned approximately 20 cm from a low-speed cylindrical collector, rotating at approximately 10 rpm. The atmospheric conditions during all electrospinning sessions were controlled by an air handling unit to an average temperature of 30°C, and a relative humidity between 60-80%. Each sample was made using 12 ml of solution, resulting randomly oriented nanofibres with an aerial weight approximately 6-10 g/m^2. The variations in aerial weight were caused by differences in deposition area width as a result of the voltage variation.

All other membranes were fabricated at the University of Sheffield, and were synthesised by pumping the polymer solutions to the spinneret at a flow rate of 1500 - 3000 μl/hour. The spinneret was charged between 16 and 25 kV, positioned between 14 and 21 cm from a static collector plate. The atmospheric solutions at the University of Sheffield were unable to be controlled, but the relative humidity remained within 31 - 40% RH, and temperature ranged from 19 - 24°C. The variation in both humidity and temperature was caused by changes in the ambient conditions over the different days on which the spinning occurred. The variation in humidity and temperature over the course of the synthesis of each material was significantly lower, with humidity varying by a maximum of 0.7% RH, and temperature varying by a maximum of 0.6°C. The electrospinning conditions used to produce the membrane samples reported here are summarised in Table 1.

Membrane samples were cut for acoustic testing using a form or sharp scissors. Sharp scissors were found to be a better tool for cutting the membrane samples. Due to the thinness and lightness of some of the membranes the form was often tearing and delaminating the membrane rather than cutting a precise circle from it.

The melamine foam substrate was cut to size using a 45mm ID in-house manufactured hole saw on a pillar drill. The hole saw was made to the correct internal diameter and did not feature serrated edges which would tear foam.

2.1. Acoustical measurements

The acoustical properties of the fibrous membranes listed in Table 1 were measured at the University of Sheffield in the 45 mm impedance tube [3] in the presence of the melamine foam substrate. This arrangement is shown schematically in Fig. 1 and operates in accordance with the ISO 10543-2 [4]. The thickness of the foam substrate was h_m =16 mm. The density, ρ_m, and total porosity, ϕ_t, of melamine foam were measured non-acoustically. The total porosity of melamine foam relates to the proportion of air in the open and closed pores. The acoustic porosity (proportion of open, interconnected pores which contribute to the measured acoustical properties), ϕ_m, flow resistivity, σ_m, and standard deviation in pore size distribution, σ_s, of melamine foam were inverted by minimising the difference between the measured and predicted complex reflection coefficient spectra. The 3-parameter model for

Table 1
Electrospinning conditions for the synthesis of the membranes used in this work. The membranes marked with I were obtained through collaboration with NXTNano (OK, USA), and are commercial materials so details of their synthesis could not be shared.

Membrane	Concentration (%w/w)	Voltage (kV)	Collector Distance (cm)	Flow rate μL/H)
15 kV PMMA	20	15	20	600
21 kV PMMA	20	21	30	1500
CD1	12.5% PCL	16	16	1000
CD2	12.5% PCL	16	18	1000
CD3	12.5% PCL	16	22	1000
I	20% PET	20	16	2000
II	20% PET	25	14	2000
III	20% PET	18	14	2500
V1	12.5% PCL	16	20	1000
V2	12.5% PCL	18	20	1000
5gsm TPU	+	+	+	+
11gsm TPU	+	+	+	+
THF_C(ii)	12.5% PCL	17	20	1500
THF_A	12.5% PCL	16	20	750
THF_C	12.5% PCL	17	20	1000
THF_F	12.5% PCL	18	20	1000
CF_B	12.5% PCL	16	20	1000
CF_C	12.5% PCL	16	20	1000
FR2	12.5% PCL	16	20	1250

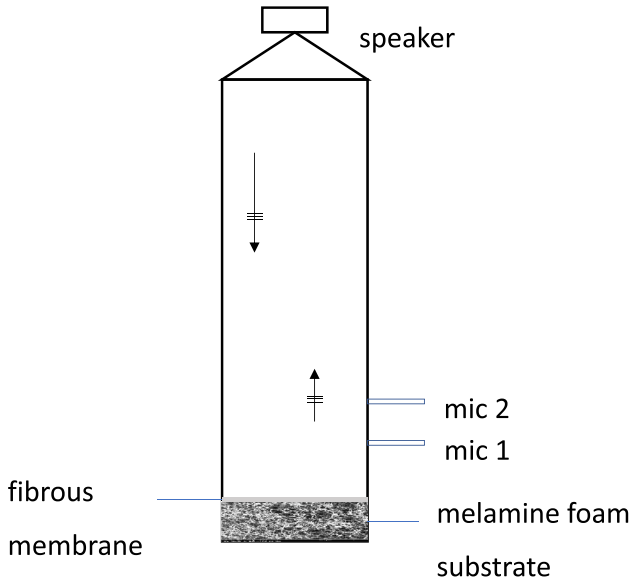

Fig. 1. Experimental arrangement in the impedance tube used to study the acoustical properties of fibrous membranes in accordance with ISO 10534-2 [4].

the acoustical properties of porous media [5] was used to fit the measured complex acoustic reflection coefficient of melamine foam. The inversion procedure is described in ref. [6]. It was based on minimising the difference between the predicted acoustic reflection coefficient and data measured with the impedance tube operating within the frequency range 200 to 2500 Hz. The flow resistivity of the foam was calculated from:

$$\sigma_m = 8\eta\alpha_\infty/(\bar{s}^2\phi_m)e^{6(\sigma_s \ln 2)^2} \quad (1)$$

where η is the dynamic viscosity of air, $\alpha_\infty = e^{4(\sigma_s \ln 2)^2}$, is the tortuosity and $\bar{s}$is the median pore size. Fig. 2 shows the comparison between the measured and predicted complex reflection coefficient for melamine foam. The mean relatively error was within 1%. Table 2 presents a summary of these non-acoustical parameters for melamine foam.

The use of the substrate meant that the key consideration when mounting the membranes to the melamine substrate was to avoid drastically changing the properties of either the membrane or the substrate. The use of a contact adhesive to secure the membrane would not have been suitable as it would affect the rigid structure of both membrane and substrate, and potentially introduce structural vibration affects to the acoustic analysis. Using pins to hold the membrane in place would not have been suitable either as the pins would result in holes dramatically reducing the effective flow resistivity of the membranes, as the size of the holes would be larger than the average pore size present in the membrane. Two approaches were used to secure the membranes to the melamine substrate, both of which had to be non-permanent and avoid changing the material properties.

The first approach involved cutting the membrane oversized and using the mating faces of the impedance tube to keep the membrane taut and in place on the surface of the melamine, as shown in Fig. 3. The second approach, shown in Fig. 4, was to prepare an oversized membrane sample and then attempt to wrap it around the substrate. The friction between the tube and the melamine would then keep the membrane held in place, but it did not guarantee the complete absence of a circumferential airgap. In all cases, each sample membrane was mounted using the first approach. Where there was insufficient material, due to difficulties in synthesis and preparation, samples were cut to the size of the melamine and placed on the surface of the melamine. This occurred for samples CD1-3.

2.2. Optical imaging and analysis

Once all the randomly orientated nanofibre membranes were electrospun and dried, they were analysed in a TESCAN MIRA II scanning electron microscope (SEM). For each membrane, images were acquired at identical magnifications, then using the built-in

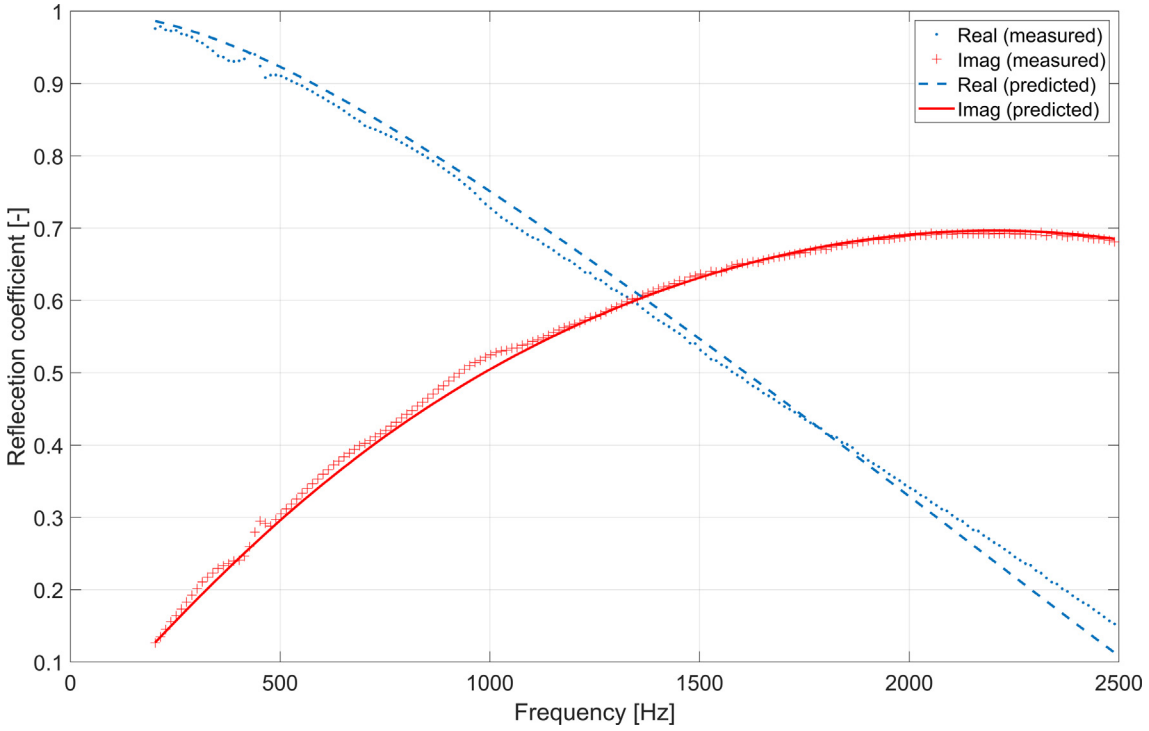

Fig. 2. A comparison between the measured and predicted real and imaginary parts of the complex reflection coefficient for the 16 mm layer of the melamine foam substrate.

Table 2
Material properties of the melamine foam substrate used to mount the membranes for acoustic testing.

Substrate	h_m[mm]	ρ_m[kg/m^3]	ϕ_t[−]	ϕ_m[−]	$\bar{s}$[μm]	σ_s[−]	σ_m[Pa•s/m^2]
Melamine	16	11.00	0.97	0.78	121	0.121	1.36x10^4

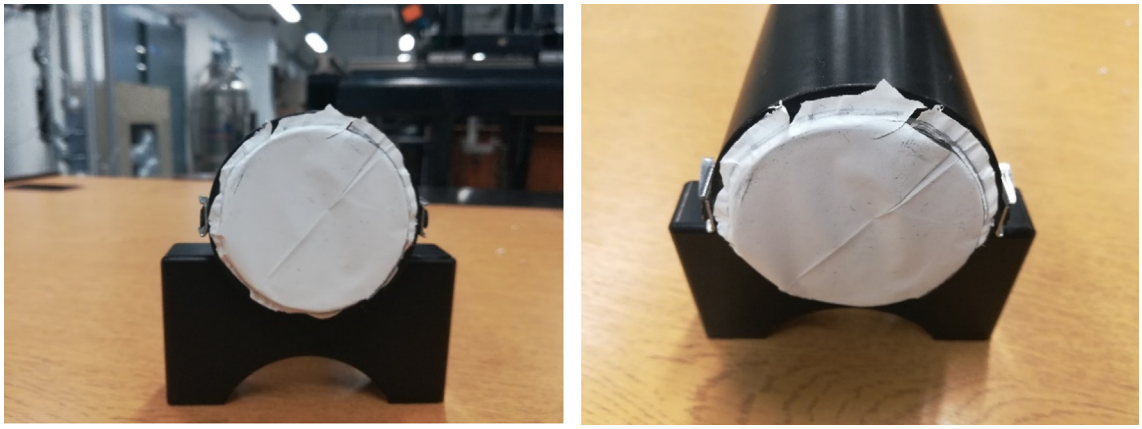

Fig. 3. A membrane is cut oversized and placed over the substrate in the tube. When inserted the mating face of the impedance tube ensures a tight seal.

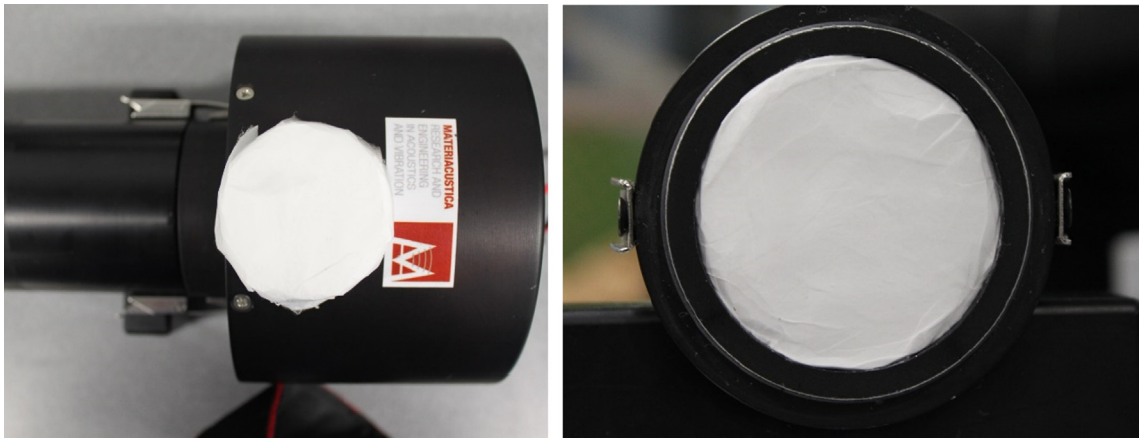

Fig. 4. A membrane can be seen wrapped around a 45 mm diameter melamine substrate. The folds of the membrane can also be seen as straight sections relative to the curve present in other areas.

software, diameter measurements of at least 50 nanofibres were taken to produce histograms for the fibre diameter, average fibre diameter, $\overline{d}$, and statistical errors. Images of these materials can be downloaded from this Google Drive folder which contains supplementary material for this paper [7].

Measuring nanofibrous membrane thickness is not a straightforward task. Nanofibrous membranes are relatively soft and very thin, so the use of a standard micrometer yields large errors due to the materials compressibility. In this work the membrane thickness, h_{nf}, was measured via SEM. Fig. 5 shows an example SEM micrograph of the cut edge of a CD1 membrane made of nanofibres. Cutting nanofibres poses similar challenges to using a micrometer. It was found that significant tearing, delamination, and rounding of the sample was occurring making measuring the edge thickness particularly challenging. Despite all the care taken to ensure a clean cut, it is not obvious from the micrograph shown in Fig. 5 what is the actual thickness of this membrane. This means that depending where on the micrograph is taken one can incur up to 100% error in the membrane thickness estimate. To minimise tearing and delamination the membrane samples were placed into Lecia OCT compound/tissue freezing medium and rapidly frozen using liquid nitrogen. The frozen membranes, now encased in the solid OCT medium, were mounted onto a stub and placed in a Leica CM1860 UV cryostat at a temperature of -20°C. 100 μm slices were shaved off the encased samples until it could be seen that the sample had been reached. The encased samples were then removed from the stub, turned through 180° and remounted onto the stub. The shaving procedure was repeated until it was apparent that the representative membrane surface had been reached and a clean edge had been achieved. Cuts were made at both ends of the sample to ensure that two clean edges were present on the membrane, making identification of the clean edges easier when mounting and viewing the sample via SEM. The resin was then dissolved by placing the samples in de-ionised water and the sample dried prior to being mounted for SEM.

Two measurement methods were used to measure the sample thickness: (i) tilting the stage of the SEM to try to get an edge in view; and (ii) attempting to 'fold' a part of the membrane up to allow for a clear view of the edge. In the first method the membrane sample was cut and placed on an SEM stub, then placed into

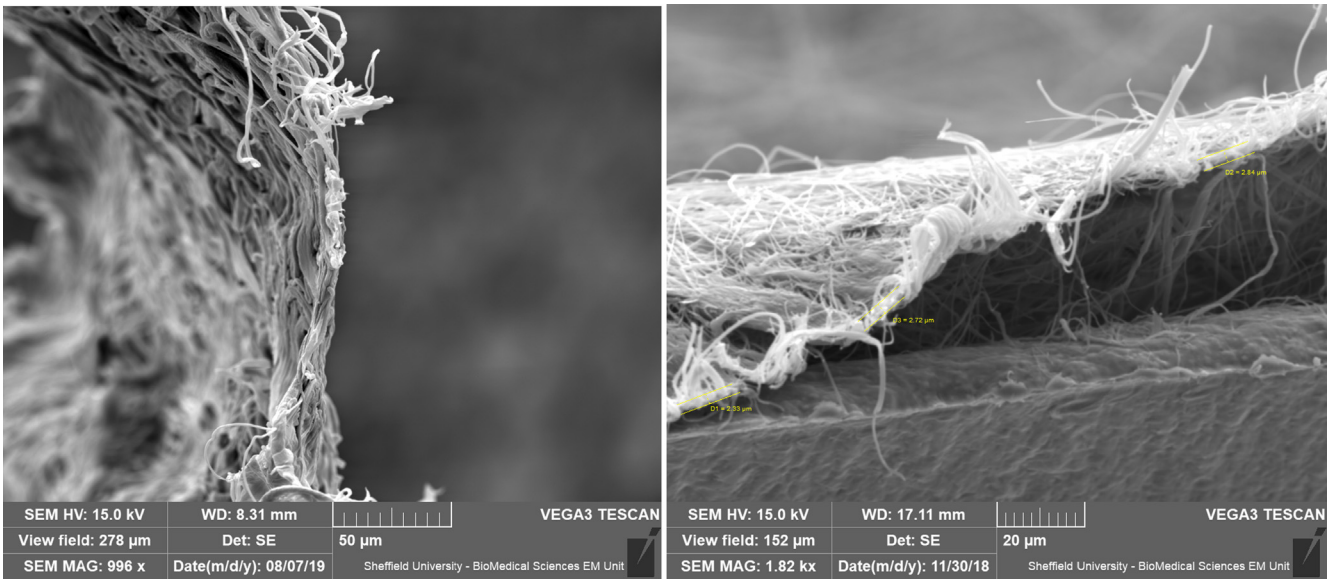

Fig. 5. Variation in edge thickness of sample CD1 due to edge rolling, uneven cuts, and natural variation due to the random nature of deposition. The darker grey lower object in the right (R) image is the Leit-C Plast used to prop up the sample.

the TESCAN MIRA II. The stage was tilted to a 45° angle, enabling an edge-on view on the sample from which thickness measurements were taken. 45° was the maximum attainable stage angle in the TESCAN MIRA II as any further angle could have caused potential collisions between the stage and lens due to the low working distances required. The measurement program used was the in-built TESCAN program, which does account for any parallax errors introduced by tilting the stage. Despite this, it still proved challenging to obtain robust measurements as it was not always apparent where the edge of the sample actually ended and adhesive backing of the stub actually began.

The second method involved the folding of one side of the sample so that it sits at a 90° angle to the rest of the sample on an SEM stub. The second method was used preferentially where membrane samples had sufficient stiffness to stay vertical without significant edge rolling. In this way problems associated with parallax errors in the microscope and its software caused by tilting the stage were eliminated. Leit-C Plast (Agar Scientific, Essex, ENG) was formed into a rectangular shape and used to support the vertical part of the membrane. Fig. 6 shows the cleanliness of the edge attainable using this method in the case of an 11gsm TPU 19.37 µm thick nanofibrous membrane. Whilst this method was reliable for membranes typically greater than 20 µm thickness (e.g. see Fig. 6), for thinner membranes or membranes with a lower stiffness there were issues with thickness measurements by SEM, with the edges of the membranes rolling over or curling once placed on the SEM stub. Our experience shows that, even with good practice and improved methods, there is still a need for further development of current techniques, or the utilisation of new techniques to obtain accurate thickness measurements of nanofibrous membranes.

2.3. Density and porosity measurements

The bulk density of the membrane was then calculated from their measured weight, m, and membrane thickness, h_{nf}. The membranes were weighed using an Ohaus AX124 analytical balance and the thickness was taken from SEM measurements as above. Density was then calculated from the standard mass of the materials over its volume. The total porosity was estimated for the nanofibrous membranes using their material density, ρ_b, and fibre density, ρ_f, according to the following equation:

$$\phi = 1 - \frac{\rho_b}{\rho_f} \tag{2}$$

The error in the membrane thickness measurement had a strong implication on the accuracy of the membrane density and porosity calculations which was likely to be high for the membranes listed in Table 1.

2.4. Air flow resistivity measurements

Air flow resistivity is a key parameter which controls the acoustical properties of porous media [6]. It was not possible to measure the airflow resistivity of the membranes directly using the airflow resistivity equipment at Sheffield that conforms to the standard direct-flow method [8]. This was because the air resistivity of the membranes was extremely high causing the membranes to be inflated and ultimately ruptured under the pressure of the airflow. Attempts to weigh the membranes down with melamine foam samples to reduce the inflation issue did not prove successful, nor did placing melamine foam samples in front of the membranes to reduce the pressure – in both cases the membranes still inflated. Therefore, this parameter was estimated from the impedance tube data on the acoustic complex reflection coefficient using the parameter inversion similar to that used to determine the flow resistivity of the melamine foam substrate. The 3-parameter model for the acoustical properties of porous media [5] was used to fit the measured complex acoustic reflection coefficient of nanofibrous membrane placed on the top of melamine foam substrate (see Fig. 1). The inversion procedure described in ref. [6] was based on minimising the difference between the predicted acoustic reflection coefficient and data measured with the impedance tube in the frequency range between 200 and 2500 Hz. The non-acoustical parameters inverted from acoustical data were used to estimate the effective (combined) flow resistivity of the membrane and foam stack, σ_e, from eq. (1). The effective flow resistivity of the nanofibrous membrane, σ_{nf}, was then estimated from the following equation:

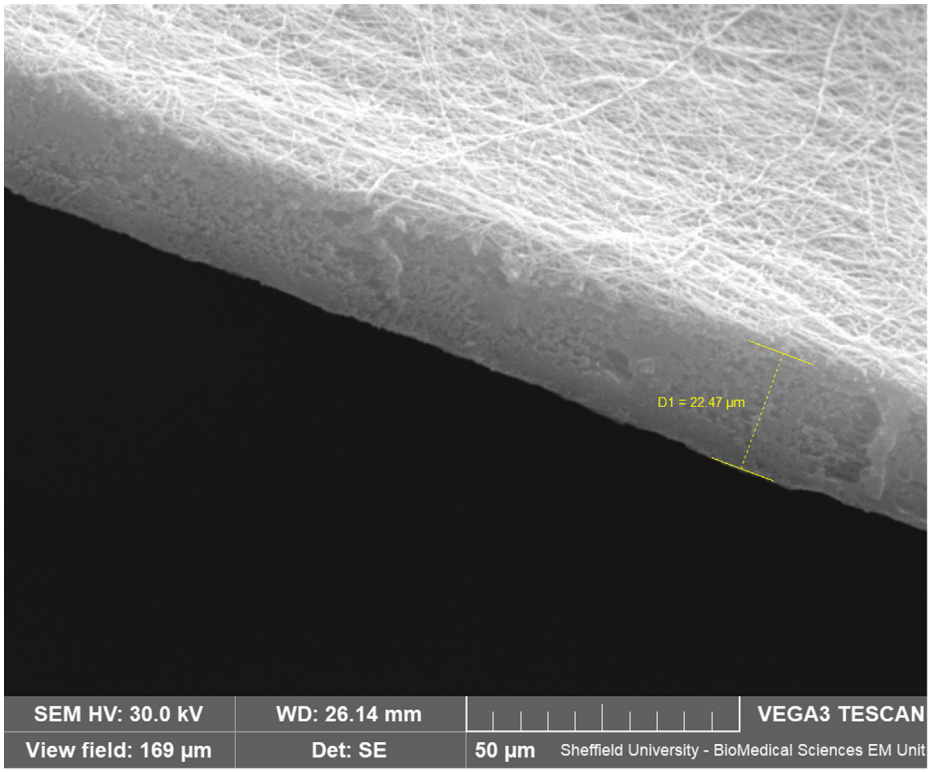

Fig. 6. A SEM micrograph of the edge of an 11gsm TPU nanofibrous membrane prepared using a cryostat and mounted using Leit-C Plast.

$$\sigma_{nf} \cong \frac{(\sigma_e - \sigma_m)h_m}{h_{nf}}, \tag{3}$$

where $h_{nf}$is the membrane thickness. Eq. (3) assumes that $h_{nf} \ll h_m$ and that the total flow resistivity of the nanofibrous membrane and melamine foam arrangement, if measured in accordance with the ISO9053 [8], is:

$$\sigma_e = \frac{1}{V}\frac{\Delta P_m + \Delta P_{nf}}{h_m + h_{nf}}, \tag{4}$$

where ΔP_m and ΔP_{nf} are the pressure drops over the melamine foam substrate and membrane, respectively, and V is the air flow velocity through the stack.

3. Results

Fig. 6 illustrates the effect of a 22 µm thick, 15 kV PMMA nanofibrous membrane on the complex reflection coefficient, r, of the melamine foam substrate. The continuous lines correspond to the predictions by the model detailed in ref. [5] and markers correspond to the measured data. The presence of a very thin nanofibrous membrane causes a significant reduction in the real and imaginary parts of the reflection coefficient. This effect is explained by the increase in the real part of the surface impedance of the melamine foam substrate when the thin, nanofibrous layer is added on the top it. This effect is well explained in ref. [9] (see eq. (7) in ref. [9]) and it is caused by the massive flow resistivity of nanofibres. Effectively, the surface acoustic impedance of a stack of these two layers is:

$$Z_s \approx \sigma_{nf} h_{nf} + Z_m coth(-ik_m h_m), \tag{5}$$

where Z_m and k_m are the characteristic acoustic impedance and wavenumber in melamine foam and $i = \sqrt{-1}$. The quantities $Z_m = \mu + i\nu$ and $k_m = \theta + i\gamma$ are complex and frequency dependent. Because the acoustic reflection coefficient and real and imaginary parts of the surface impedance are related as:

$$r = \frac{\mu^2 - z_0^2 + \nu^2}{(\mu + z_0)^2 + \nu^2} + \frac{2i\nu z_0}{(\mu + z_0)^2 + \nu^2}, \tag{6}$$

then the minimum in the reflection coefficient, $r = r_R + ir_I$, is achieved when the real part of the surface impedance, μ, is close to the impedance of air, z_0,and its imaginary part, ν, is small with respect to it, $z_0 = \rho_0 c_0$. Here ρ_0, c_0 are the density and sound speed in air, respectively. Unfortunately, the imaginary part of a relatively thin layer of foams such as 16 mm thick melamine foam used in our experiments is relatively large in comparison with z_0. This is because the acoustic wavelength, $\lambda \approx 2\pi/\theta$, is relatively large in comparison with h_m. Therefore, the only way to reduce the reflection coefficient and to increase absorption of this foam is to increase the real part of the surface impedance to make it comparable with the imaginary part. The acoustic absorption coefficient is defined as:

$$\alpha = 1 - |r_R + ir_I|^2, \tag{7}$$

which means that both the real and imaginary parts of the complex reflection coefficient contribute to the value of absorption coefficient. Therefore, the reduction in both real and imaginary parts of the reflection coefficient is important to achieve a higher value of the absorption coefficient. This reduction can be realised by adding a nanofibrous membrane to the foam as illustrated in Fig. 7.

The effect the 15 kV PMMA membrane on the acoustic absorption coefficient and surface impedance of the 16 mm thick melamine foam is illustrated in Fig. 8 (top). At some frequencies, *e.g.* 2000 Hz, the increase in the absorption coefficient is close to 75%. This increase is achieved by adding a 22 µm thick nanofibrous membrane to the top of melamine foam. The addition of this mem-

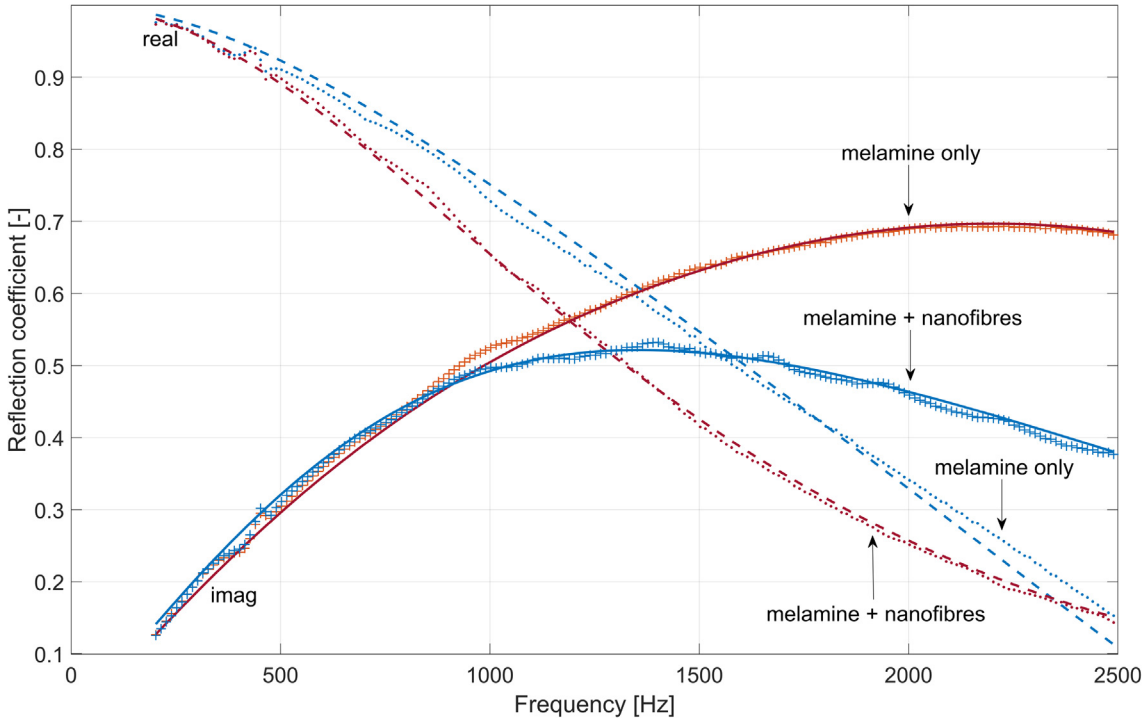

Fig. 7. The effect of nanofibrous membrane on the real and imaginary part of a 16 mm thick layer of melamine foam. Lines correspond to the theoretical fit, dots and crosses correspond to the measured data.

brane results in over 100% increase in the real part of the surface impedance (110% at 2000 Hz) which means that the real part of the surface impedance of this material becomes comparable to that of air (see Fig. 8 (bottom)). There is also a small drop in the imaginary part of the surface impedance which contributes to extra absorption, but this change is relatively small (22% at 2000 Hz) and it is likely to be caused by the membrane vibration rather than its high resistance (see Fig. 8 (bottom)).

Table 3 presents a summary of the key non-acoustical parameters of the nanofibrous membranes studied in this work. These parameters are the mean fibre diameter, density, porosity, effective flow resistivity of the membrane/melamine foam system and flow resistivity of the nanofibre. This table also lists the Knudsen number which is defined as:

$$K_n = \frac{l}{\overline{d}}, \tag{8}$$

where $l = 68$ nm is the mean free path for air taken at room temperature and normal atmospheric pressure. Table 3 also presents the values of the nondimensional parameter which shows the relation between the flow resistivity of nanofibres and mean fibre diameter, $\sigma_{nf}\overline{d}^2/\eta$.

According to the Kozeny-Carman model [10] the relation between the flow resistivity and fibre diameter is:

$$\frac{\sigma\overline{d}^2}{\eta} = \frac{180(1-\phi)^2}{\phi^3}. \tag{9}$$

The Kozeny-Carman model works well to predict the flow resistivity, σ, of highly porous media composed of fibres with the diameter of a few microns [10]. However, it is interesting to check if it also works for fibrous media made of nanofibres. To the best of our knowledge this has not been done before for flow velocities through the fibres which are comparable with the acoustic velocity in the audible range.

Let us denote the left- and right-hand parts of eq. (9) as:

$$f_1\left(\sigma, \overline{d}\right) = \frac{\sigma\overline{d}^2}{\eta}, \tag{10}$$

and

$$f_2(\phi) = \frac{180(1-\phi)^2}{\phi^3}, \tag{11}$$

respectively. We can call these two functions the flow resistivity, f_1, and porosity, f_2, terms, respectively.

The work by Umnova et al [11] suggests that the flow resistivity of in eqs. (10) and (11) needs to be compensated for the so-called no-slip effects when the fibres diameter, $\overline{d}$, becomes comparable to mean free path, l. According to this work the flow resistivity of nanofibres compensated for no-slip condition is (eq. (46) in [11]):

$$\sigma_\perp = \frac{\sigma}{1+\frac{4K_n}{1+2K_n}F\left(\phi_{nf}\right)}, \tag{12}$$

where

$$F\left(\phi_{nf}\right) = \frac{\phi_{nf}^2}{-2\ln\left(1-\phi_{nf}\right)-2\phi_{nf}-\phi_{nf}^2} \tag{13}$$

and σ is predicted by eq. (9). It is logical to assume that functions (10) and (11) should be equal if eq. (9) holds for nanofibres.

Let is now use eqs. (10)-(13) and data from Table 3 to check how eq. (9) holds for nanofibres. Fig. 9 graphically illustrates the dependence of these functions on the Knudsen number. The triangles in this Fig. 9 are the experimentally determined values of the flow resistivity of nanofibres which are normalized by the mean fibre diameter and dynamic viscosity. The circles are the values of function (11) predicted for the measured porosity of nanofibres. If eq. (9) were to hold, then the two sets of data shown in Fig. 9 would be close to the solid black line which corresponds to the value of $f_2(0.8)$; $\phi_{nf} = 0.8$ is a typical value of porosity fibrous

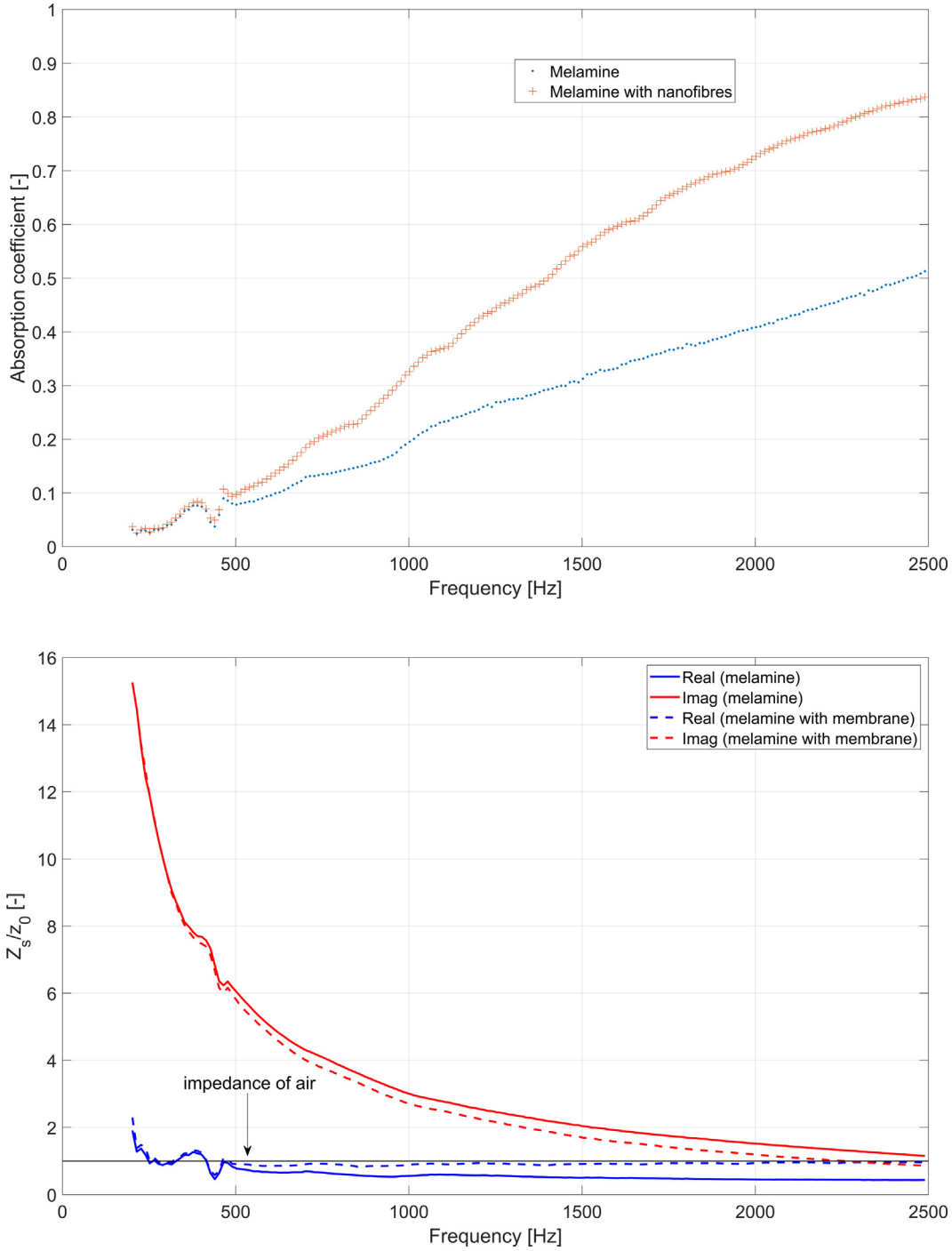

Fig. 8. The effect of nanofibrous membrane (15 kV PMMA, 22 μm thick) on the acoustic absorption coefficient (top) and complex surface impedance (bottom) of a 16 mm thick layer of melamine foam.

media made from relatively large fibres (e.g. membranes CD1-CD3 in Table 3). According to Fig. 9 this seems only the case for fibres with relatively large mean diameters, i.e. for $K_n \approx 0.02$. As the fibre diameter decreases, the difference between the values of $f_1\left(\sigma_{nf}, \overline{d}\right)$ and $f_2(\phi_{nf})$ becomes greater. The flow resistivity of nanofibres decreases with an increase in K_n. On the other hand, the function $f_2(\phi_{nf})$ grows with an increase in K_n. This suggests that equation (9) no longer holds for $K_n > 0.02$ or for smaller fibre diameters. The compensation for nonslip conditions (eqs. (12) and (13)) does not explain accurately the drop in the flow resistivity of nanofibres with an increase in K_n (stars in Fig. 9). The stars in Fig. 9 show that the difference between the flow resistivity compensated for noslip conditions, $\sigma_{\perp}$, and measured flow resistivity, σ_{nf}, becomes more than one order of magnitude when the Knudsen number becomes greater than 0.1.

Table 3
Summary of the key non-acoustical parameters of nanofibrous membranes studied in this work.

	Average membrane thickness,h_{nf}	Average fibre diameter,$\bar{d}$	Knudsen number,K_n	Membrane porosity,ϕ	Effective flow resistivity of melamine foam with membrane,σ_e	Flow resistivity of membrane,σ_{nf}	$\sigma_{nf}\bar{d}^2/\eta$
Membrane	[μm]	[nm]	[–]	[–]	Pa s m^{-2}	MPa s m^{-2}	[–]
CD1	5.77	2880	0.024	0.80	27200	37.7	17.28
CD2	7.84	3630	0.019	0.81	28400	30.2	21.99
CD3	5.41	2560	0.027	0.70	20100	19.2	6.96
15kV PMMA	22.17	440	0.155	0.39	56000	30.6	0.33
21kV PMMA	32.38	390	0.174	0.31	62600	24.2	0.20
I	19.02	401	0.170	0.25	23700	8.50	0.08
II	12.1	340	0.200	0.34	20600	9.26	0.06
III	12.4	243	0.280	0.38	24200	13.7	0.04
V1	10.99	3190	0.021	0.74	23700	14.7	8.27
V2	12.75	2500	0.027	0.66	23400	12.3	4.25
5gsm TPU	19.54	409	0.166	0.35	21700	6.63	0.06
11 gsm TPU	19.37	281	0.242	0.37	29700	13.3	0.06
THF_Cii	11.87	1052	0.065	0.40	32800	25.9	1.58
THF_A	12.15	1774	0.038	0.35	31900	24.1	4.19
THF_C	10.87	1334	0.051	0.38	22100	12.5	1.23
THF_F	12.56	512	0.133	0.50	25700	15.4	0.22
CF_B	12.21	1606	0.042	0.31	46900	43.6	6.22
CF_C	12.16	1398	0.049	0.25	24700	14.6	1.58
FR2	11.33	2590	0.026	0.65	25900	17.4	6.44

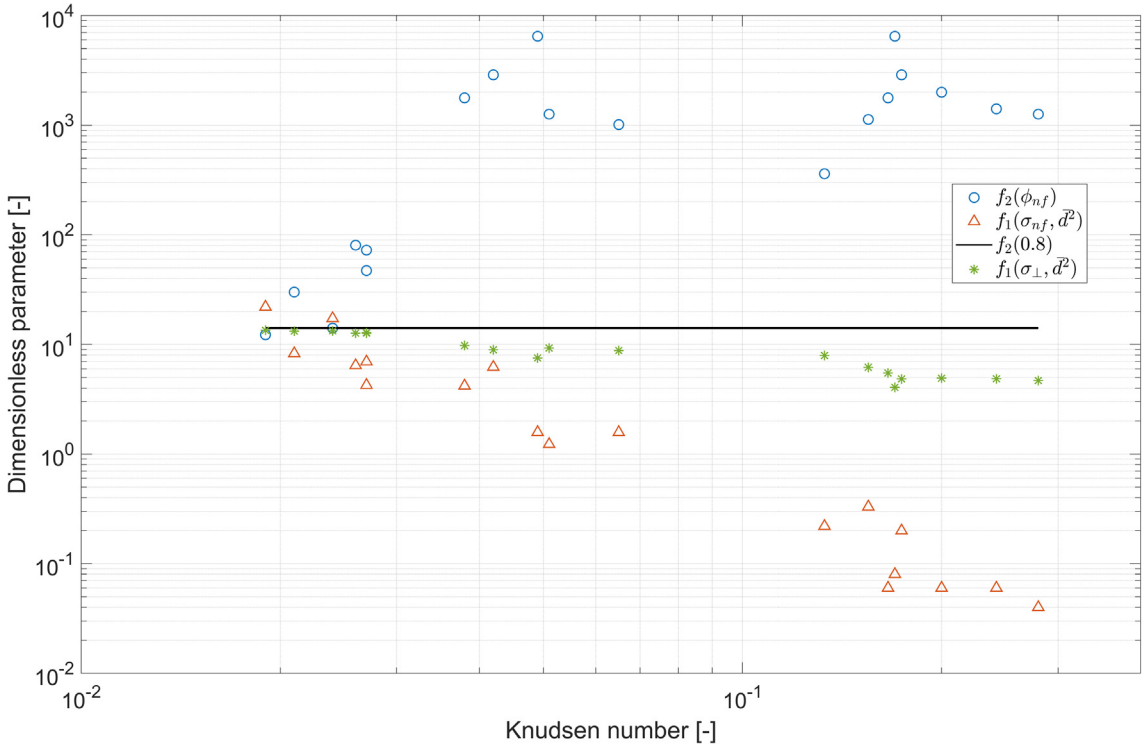

Fig. 9. The normalised flow resistivity and porosity terms in the Kozeny-Carman equations predicted for the parameters of nanofibrous media listed in Table 3. The markers graphically illustrate the dependence of functions (10) and (11) (i.e. left and right parts of the Kozeny-Carman equation (eq. (9)) on the Knudsen number. The solid line shows the value of the function f_1 calculated for a typical nanofibre membrane porosity of $\phi = 0.8$.

4. Conclusions

In this work a range of nanofibrous membranes were manufactured and their acoustical and related non-acoustical properties were studied systematically, perhaps for the first time, using a standard laboratory setup and classical models for sound propagation in porous media. The novelty of this work is three-fold. Firstly, it used a robust theoretical model to explain the observed acoustical behaviour of thin nanofibrous membranes placed on a foam substrate. Secondly, it used the acoustical data to estimate the actual flow resistivity of nanofibres. Thirdly, it demonstrates that a classical model for the flow resistivity of fibrous media does not work when the Knudsen number becomes greater than 0.02, i.e. then the diameter of nanofibres becomes comparable with the mean free path.

This research also show that the prediction of the acoustical properties of this seemingly simple system is far from easy. Our findings suggest that a classical model such as that proposed by

Kozeny and Carman cannot be used to predict the flow resistivity of nanofibres. For these materials the behaviour of the flow resistivity and porosity terms in eq. (9) differs significantly by a few orders of magnitude from that expected from porous media made of fibres which are larger than 2-3 μm. It seems that compensation for no-slip effects (suggested in Umnova *et al* [11]) does not explain sufficiently the drop in the flow resistivity of nanofibres estimated from our acoustical data.

There can be a few reasons for this behaviour. Firstly, the effect of circumferential gap on the quality of acoustical data obtained with the impedance tube experiment is not fully understood when dealing with such highly resistive media. Our previous work [12] suggests that a circumferential gap which width is comparable to the thickness of the nanofibrous membrane can result in 1-2 orders of magnitude reduction in the measured flow resistivity. This gap is difficult to eradicate or estimate accurately in the standard impedance tube experiment. Secondly, the thickness of these membranes is comparable with the thickness of the viscous boundary layer (eq. 6.4.31) in [15]):

$$\delta_v = \sqrt{\frac{\eta}{\omega\rho_0}}, \tag{15}$$

where ω is the angular frequency of sound. The viscous boundary layer thickness in the frequency range presented in Figs. 6 and 7 (200 – 2500 Hz range) will vary from 110 μm to 31 μm. This is larger than or comparable to the thickness of the nanofibrous membranes studied in this work (see Table 3). This effect is not accounted by classical flow resistivity models, e.g. the Kozeny-Carman model (eq. (9)), or acoustical prediction models, e.g. [5]. Thirdly, as the fibre diameter decreases to form a network of nanopores, sorption effects are likely to become important [13]. Therefore, it is unclear if a Kozeny-Carman-type model that is based on the Darcy law is actually valid to predict accurately the resistance of these tiny fibres to the direct flow of air. These effects are not accounted for in the models adopted in this work. There was also a high uncertainty in the membrane thickness measurement and the degree of uniformity in the arrangement of nanofibres was not fully understood. These factors could also affect our findings.

It can also be suggested that the ISO 10534-2 [5] setup needs to be redesigned to enable accurate measurements of the acoustical properties of nanofibrous membranes. The new setup must control the circumferential airgap with a micron precision to ensure that it is comparable to the membrane pore size which is usually less than a micrometre. The new setup should also enable the measurement of the structural vibration of the membrane or minimize it. This vibration can be caused by the incident sound field and it is difficult to accurately account for with a model [12]. Also, the existing ISO 9053 [8] setup is not suitable to measure the flow resistivity of nanofibrous membranes. Efforts have been made to develop specialised setups for this purpose, *e.g.* [14], but these are designed to operate at flow velocities which are much greater than that expected from an incident sound wave in an audible range.

Declaration of Competing Interest

The authors declare that they have no known competing financial interests or personal relationships that could have appeared to influence the work reported in this paper.

Acknowledgement

The authors would like to thank the EPSRC, United Kingdom, grant numbers EP/N006372/1 and EP/L016281/1, and Revolution Fibres Ltd, New Zealand, for supporting the work reported here.

References

[1] Kalinova K., Nanofibrous Resonant Membrane for Acoustic Applications, J Nanomat 2011; Article ID 265720. https://doi.org/10.1155/2011/265720
[2] A. Rabbi K. Nasouri A. Mousavi Shoushtari A. Haji Fabrication of Electrospun Polyacrylonitrile Nanofibres for Sound Application, Proc 6th TEXTEH Int. October 2013 Conf., Bucharest, Romania
[3] Materiacustica SRL, http://www.materiacustica.it/mat_UKProdotti_3Mics.html, [Last accessed on 1 September 2020].
[4] ISO10534-2:2001. Determination of sound absorption coefficient and impedance in impedance tubes, Part 2: Transfer-function method International organization for standardization 2001 Geneva, Switzerland
[5] Horoshenkov KV, Hurrell A, Groby J-P. A three-parameter analytical model for the acoustical properties of porous media. J Acoust Soc Am 2019;145(4):2512–7. https://doi.org/10.1121/1.5098778.
[6] Horoshenkov KV. A review of acoustical methods for porous material characterisation. Int J Acoust Vib 2017;22(1):92–103. https://doi.org/10.20855/ijav.2017.22.1455.
[7] Supplementary data, including SEM micrographs, figures, and MatLab code. https://drive.google.com/drive/folders/1uDEpVQRIWe2ZcCYWQuhiDioteuxhheD-?usp=sharing [Last viewed on 1 October 2020].
[8] ISO 9053:1991. Acoustics - Materials for acoustical applications - Determination of airflow resistance International organization for standardization 1991 Geneva, Switzerland
[9] Chevillotte F. Controlling sound absorption by an upstream resistive layer. J Appl Acoust 2012;73(1):56–60. https://doi.org/10.1016/j.apacoust.2011.07.005.
[10] Pelegrinis MT, Horoshenkov KV, Burnett A. An application of Kozeny-Carman flow resistivity model to predict the acoustical properties of polyester fibre. J Appl Acoust 2016;101:1–4.
[11] Umnova O, Tsiklauri D, Venegas R. Effect of boundary slip on the acoustical properties of microfibrous materials. J Acoust Soc Am 2009;126(4):1850–61.
[12] Hurrell A., Acoustical properties of polymeric fibres and their characterisation. PhD Thesis, University of Sheffield. March 2020. http://etheses.whiterose.ac.uk/26459/1/AHurrell_Thesis_Final.pdf [Last accessed on 1 September 2020].
[13] Venegas R, Boutin C. Acoustics of sorptive porous materials. Wave Motion 2017;68:162–81. https://doi.org/10.1016/j.wavemoti.2016.09.010.
[14] Biana Y, Zhanga L, Chena C., Experimental and modeling study of pressure drop across electrospun nanofibre air filters. Build Env 2018; 142: 244-151. https://doi.org/10.1016/j.buildenv.2018.06.021
[15] Morse PM, Ingard U. Theoretical acoustics. New York: McGraw-Hill; 1968.
[16] Hahladakis JN, Velis CA, Weber R, Iacovidou E. An overview of chemical additives present in plastics: Migration, release, fate and environmental impact during their use, disposal and recycling. Journal of Hazardous Materials 2018;344:179–99. https://doi.org/10.1016/j.jhazmat.2017.10.014.